Theoretical and Applied Fracture Mechanics 118 (2022) 103220

Contents lists available at ScienceDirect

Theoretical and Applied Fracture Mechanics

journal homepage: www.elsevier.com/locate/tafmec

Evaluation of *R*-curves and cohesive law in mode I of European beech

J.L. Gómez-Royuela [a,*], A. Majano-Majano [a], A.J. Lara-Bocanegra [a], J. Xavier [b], M.F.S.F. de Moura [c]

[a] Department of Building Structures and Physics, ETS of Architecture, Universidad Politécnica de Madrid (UPM), Avda. Juan de Herrera, 4., 28040 Madrid, Spain
[b] UNIDEMI, Department of Mechanical and Industrial Engineering, NOVA School of Science and Technology, NOVA University Lisbon, 2829-516 Caparica, Portugal
[c] Faculdade de Engenharia da Universidade do Porto, Departamento de Engenharia Mecânica e Gestão Industrial, Rua Roberto Frias, 4200-465 Porto, Portugal

ARTICLE INFO

Keywords:
Beech
Mode I
Cohesive law
Digital image correlation
FEM
Double cantilever beam

ABSTRACT

This work addresses the determination of the cohesive laws in Mode I and tangential–longitudinal (TL) crack propagation system of *Fagus Sylvatica* L. This species is one of the ever-growing and most widely used hardwood species in Europe for engineered timber products. Double Cantilever Beam (DCB) tests are performed. The strain energy release rate (G_I) is derived from the R-curves by applying the Compliance-Based Beam Method (CBBM), which has the advantage of not requiring the measurement of the crack length during propagation, but only the global load–displacement curves. The cohesive law of the material is determined from the relationship between G_I, and the crack tip opening displacement (CTOD) monitored for each specimen using Digital Image Correlation (DIC). Numerical finite element models are developed by implementing the average cohesive law through Cohesive Zone Models (CZM). An average G_I value of 0.46 kJ/m^2 is obtained for this species. The numerical load–displacement curves are consistent with the experimental results, which demonstrates the suitability of the method for the identification of the cohesive laws in beech. The fracture properties obtained are essential in the development of advanced and reliable numerical models in timber engineering design using this species.

1. Introduction

Recent studies show that the building sector contributes up to 30% of global annual greenhouse gas emissions and consumes up to 40% of all energy [1]. For this reason, the wood industry and therefore the construction of buildings with timber structure is undergoing strong growth. Part of this growth is driven by the need to provide environmentally friendly answers and, in this sense, wood is playing a very important role. The use of wood-based materials in building construction can reduce energy demand and CO_2 compared to other materials, such as steel, concrete, aluminum or brick [2–4]. Furthermore, wood is the only main building material that is a renewable resource as long as it is managed sustainably [5]. This interest in wood highlights the need for research to better understand its mechanical behavior. From a technical point of view, it is necessary to advance and deepen in the characterization of the material properties in order to address the design of timber structures in a safe way and develop advanced and reliable numerical models, which involves the study of the fracture behavior.

In the last decade, the use of hardwood species as a raw material for timber structures is gaining momentum over softwoods due to their advantages in term of mechanical performance and natural durability. Currently, beech wood (*Fagus sylvatica* L.) is one of the most widely used hardwoods for timber structures in Europe [6]. Therefore, predicting its fracture behavior becomes necessary, especially in design situations where brittle failures may occur, such as timber connections loaded perpendicular to the grain. For this particular case, Eurocode 5 [7] proposes a splitting resistance verification based on the fracture mechanics approach. The code expression derives from considering a critical fracture energy parameter, which was empirically calibrated based on several experimental studies on softwoods available in literature [8,9]. However, the design standard limits this verification to softwoods, so research is needed to extend its application to hardwoods, which requires determining their fracture properties.

It is well known that wood presents a high variability of elastic properties due to its natural origin. Furthermore, although it is an anisotropic material, it is widely accepted to be considered as orthotropic characterized according to three main directions: longitudinal

* Corresponding author.
E-mail addresses: joseluis.gomez.royuela@upm.es (J.L. Gómez-Royuela), almudena.majano@upm.es (A. Majano-Majano), antoniojose.lara@upm.es (A.J. Lara-Bocanegra), jmc.xavier@fct.unl.pt (J. Xavier), mfmoura@fe.up.pt (M.F.S.F.d. Moura).

https://doi.org/10.1016/j.tafmec.2021.103220
Received 21 October 2021; Received in revised form 17 December 2021; Accepted 19 December 2021
Available online 17 January 2022

(L), radial (R) and tangential (T) [Fig. 1]. This leads to consider six fracture propagation systems: RL, TL, LR, LT, RT and TR (the first letter indicates the direction normal to the crack plane and the second letter specifies the direction of crack propagation). In particular, the most relevant propagation systems from a structural point of view are RL and TL, so numerous research works focused on them in different wood species can be found in literature [10–17]. Each propagation mechanism can present a state of stresses in three different modes: mode I (in-plane tension), mode II (in-plane shear) and mode III (out-of-plane shear). Due to the low strength perpendicular to the grain of wood, the failure mode I requires special attention. In this sense, several types of experimental tests are available to characterize the mode I fracture parameters, such as the Compact Tension (CT) [18,19] the Single Edge Notched Beam (SENB) [15,20] or the Wedge Splitting Test (WST) [21,22]. One of the most suitable tests is the Double Cantilever Beam (DCB) as the specimen geometry is simple, it is able to adequately produce crack propagation, and allows the fracture energy to be determined mathematically according to the beam theory [23,24].

The complexity of wood makes that the fracture of the material is characterized by the occurrence of hardening phenomena such as multiple micro-cracks and fiber-bridging [24]. These non-linear phenomena take place in the region known as the Fracture Process Zone (FPZ) just ahead of the crack tip. Consequently, in order to adequately describe the fracture behavior of wood, it is necessary to make use of non-linear fracture theories, which were initially developed for elasto-plastic materials such as mild steel [25]. Currently, one of the simplest ways to address fracture in wood is by applying traction-crack opening laws to predefined crack propagation paths. Although wood is a strongly orthotropic material, the crack propagation pattern is usually known in advance. The first applications of this methodology correspond to the Fictitious Crack Models [26,27], today known as Cohesive Zone Models (CZM), being for the first time applied to wood in [28]. The traction-crack opening laws are considered material properties and relate the tractions with the total displacement at the crack tip. They consist of an initial branch corresponding to the elastic behavior of the material until the maximum traction is reached, followed by a softening branch describing the damage development [29]. These cohesive laws can be obtained experimentally by direct methods [11] or by inverse methods using numerical simulations [30].

The main objective of the present work is to experimentally estimate the resistance curves (*R*-curves) and the representative cohesive laws in mode I and TL crack propagation system of European beech wood (*Fagus sylvatica* L.) using DCB specimens. The *R*-curves are determined applying the Compliance-Based Beam Method (CBBM). This data reduction scheme is based on the beam theory and an equivalent crack length (a_{eq}) concept, which has the advantage of not requiring the measurement of crack growth during the test, which would be a difficult and complex task in wood. Instead, only the load–displacement curve is needed. The cohesive laws are derived directly from the relationship between the critical strain energy release rate (G_{Ic}) obtained from the R-curves, and the crack tip opening displacements (w) monitored using digital image correlation (DIC) technique. Numerical simulations by finite element models were performed to validate the experimental procedure. CZM were applied to predefined paths in the specimen geometry in order to implement the fracture mechanisms and validate the results.

2. Materials and methods

2.1. Raw material

Clear wood specimens made of European beech (*Fagus sylvatica* L.) were manufactured. All specimens were randomly cut from boards from a single log and machined in such manner that they are oriented according to the orthotropic directions (Fig. 2). Before testing, the specimens were stored at 20 °C and 65% relative humidity until equilibrium moisture content was reached. A mean density of 704 kg/m^3 and 10.5% average moisture content were measured. Constant values for the tangential modulus of elasticity E_T=832 MPa (St. Dev.=115 MPa) and for the shear modulus G_{LT}=706 MPa (St. Dev.=139 MPa) were taken from [31].

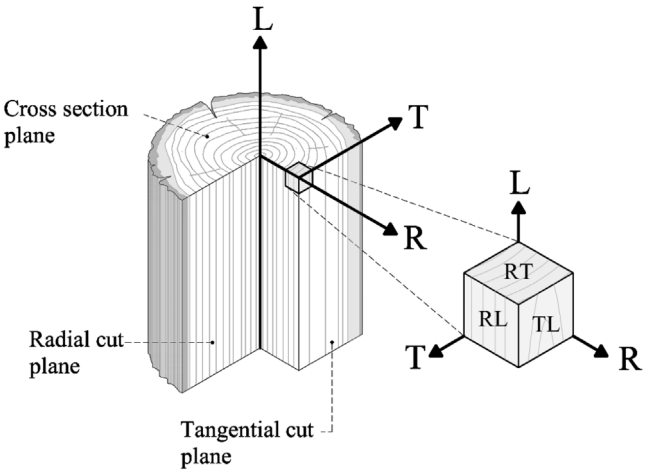

Fig. 1. Main orthotropic directions and planes in wood.

2.2. DCB test coupled with digital image correlation

In this work, seventeen DCB specimens oriented according to the TL crack propagation system as schematically represented in Fig. 2 were prepared for studying the fracture behavior in mode I of European beech. The specimens consist of small rectangular beams with nominal dimensions $L \times 2h \times B$ (250 mm × 20mm × 20mm). A notch of 1 mm thickness was machined at mid-height using a band saw. Prior to testing, this notch of initial length a_0 (100 mm) was lengthened by 1 mm using a very sharp blade to guarantee a sharped pre-crack surface before crack propagation. The pre-crack depth was controlled using a universal testing machine under displacement control of 10 mm/min. The pre-crack length was measured with a precision magnifying glass as shown in Fig. 3. A symmetrical pair of holes of 3 mm diameter were drilled at mid-height of the arm and 10 mm distance from the specimen test end (e in Fig. 2). Two steel pins of the same diameter were introduced into the holes to transfer the mode I load to the specimen. The resultant applied load was measured by a load cell of 5 kN maximum capacity. The DCB specimens were loaded by displacement control applying a constant load rate of 2 mm/min.

The DIC system ARAMIS® 3D [32] was used to record the crack tip opening displacements (Fig. 4). The device comprises two 5 megapixels resolution cameras coupled with 35 mm lens and two white light spotlights. They were calibrated using the CP20 90 × 72 calibration panel according to the target region of interest. To ensure correct focusing of the specimen surface, a field of view of 80 mm × 65mm and a distance of 400 mm between the cameras and the specimen were established. An stereo-vision angle of 25° between cameras was set. The base distance between cameras was locked at 138 mm. The shutter time and the spotlights were setup to enhance contrast and adequately lighting the specimen, avoiding insufficient or excessive light exposure. ARAMIS®3D was coupled to the universal testing machine to record synchronized data with a frequency of 1 Hz. Speckle pattern was applied on the specimen surface of interest to ensure the accuracy of the measurements using the DIC technique. This textured pattern was created in two phases. Firstly, a thin homogeneous layer of matte white paint was applied with a spray, and then a black dots pattern was projected using an airbrush. The created pattern guaranteed suitable

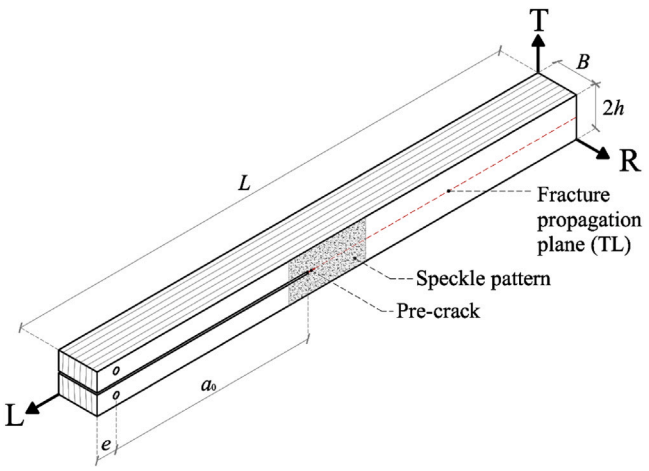

Fig. 2. Geometry of the DCB specimen.

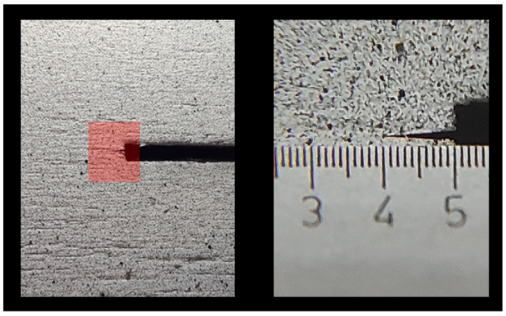

Fig. 3. Pre-crack measurement by a precision magnifying glass.

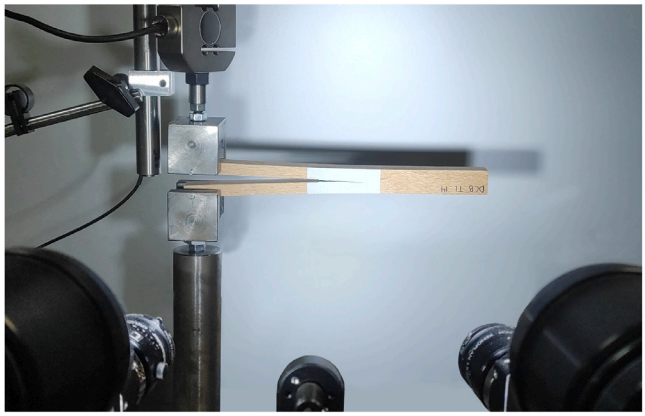

Fig. 4. DCB test set-up coupled with DIC.

contrast and granulometry of the surface according to the magnification scale of observation. Subset size of 15 × 15 pixel^2 and a subset step of 13 × 13 pixel^2 were selected for enhancing spatial resolution in a compromise with accuracy, since the DIC setting parameters can have a significant influence in the kinematics measurements [33,34].

2.3. R -curves: Compliance based beam method

The crack growth resistance curves (R-curves) describe the evolution of the strain energy release rate G_I as a function of the crack length a. A fracture process zone (FPZ) arises in the region close to the crack tip, where various toughening mechanisms take place, such as multiple micro-cracks, cracks-branching and fiber-bridging. These non-linear phenomena influence the fracture behavior of wood and therefore cannot be neglected. The R-curve is a useful tool to quantify the influence of the FPZ and obtain the critical fracture energy G_{Ic}, since this parameter is given by the plateau value of these curves.

The strain energy release rate can be obtained according to the Irwin–Kies equation,

$$G = \frac{P^2}{2B}\frac{\mathrm{d}C}{\mathrm{d}a}, \tag{1}$$

where P, B, C and a are the test load, the specimen width, the specimen compliance ($C = \delta/P$) and the crack length, respectively. It should be noted that the toughening mechanisms developing at the FPZ in wood make difficult an accurate measurement of a during testing. To avoid this problem, the Compliance-Based Beam Method (CBBM) [24] was applied in the determination of $\mathrm{d}C/\mathrm{d}a$. This methodology is based on the Timoshenko beam theory and an equivalent crack length (a_{eq}) concept. Accordingly, for a DCB test, the specimen compliance can be written as [24],

$$C = \frac{8a^3}{E_L B h^2} + \frac{12a}{5BhG_{LT}}, \tag{2}$$

where E_L and G_{LT} are the longitudinal and the shear modulus of elasticity in the LT plane, respectively. It should be noted that Eq. (2) does not take into account the stress concentrations and assumes that the rotation at the crack tip is zero, but actually this is not the case. To account for these effects, a correction to the initial crack length (Δ) is used, so that $a = (a_0 + \Delta)$, being Δ the William's correction factor [35],

$$\Delta = h\sqrt{\frac{E_f}{11G_{LT}}\left[3 - 2\left(\frac{\Gamma}{1+\Gamma}\right)^2\right]} \quad \text{where} \quad \Gamma = 1.18\frac{\sqrt{E_f E_T}}{G_{LT}}. \tag{3}$$

As mentioned before, another typical problem in wood is the variability of the elastic constants. To overcome this issue, a corrected bending modulus E_f is used for each specimen instead of E_L. The E_f value can be obtained from Eq. (2) considering the initial compliance $C = C_0$ estimated by linear regression of the $P - \delta$ curve using least squares method,

$$E_f = \left[C_0 - \frac{12\,(a_0+\Delta)}{5BhG_{LT}}\right]^{-1}\frac{8\,(a_0+\Delta)^3}{bh^3}. \tag{4}$$

Successive iterations between Eqs. (3) and (4) are performed until a convergent value of E_f is reached. It should be noted that no significant errors are made when neglecting the influence of the variability of the other elastic constants (E_T and G_{LT}) on the final value of G_I, so the average values of these constants can be used as input parameters [24]. During propagation, the current specimen compliance ($C = \delta/P$) is registered and used to obtain the equivalent crack length during crack propagation. With this aim, Eq. (2) is used to get a_{eq} as a function of C. The resultant cubic equation is solved with Matlab® software (see more details in [24]). This parameter accounts for the FPZ effects, i.e., $a_{eq} = a + \Delta + \Delta a_{FPZ}$, since the current specimen compliance reflects the influence of them. Finally, combining Eqs. (1) and (2), the energy release rate is reached according to the following expression,

$$G_I = \frac{6P^2}{2B}\left[\frac{2a_{eq}^2}{h^2 E_f} + \frac{1}{5G_{LT}}\right]. \tag{5}$$

Therefore, G_I can be determined only from the load vs. displacement data ($P - \delta$) without the need for measurements of a during the DCB test [36], being a reasonable alternative applicable to wood [11].

2.4. Cohesive law: Direct method

The cohesive laws for pure mode I loading describe the evolution of tractions as a function of the crack tip opening ($\sigma = f(w)$) and can be determined according to the following expression [37],

$$G_I = \int_0^{\bar{w}} \sigma\,(w)\,\mathrm{d}w. \tag{6}$$

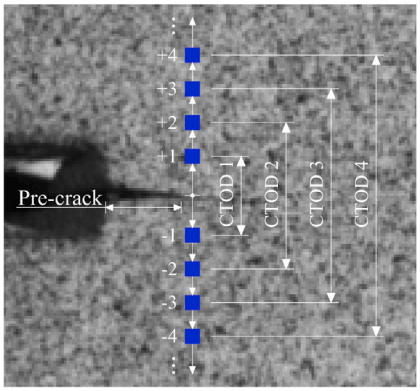

Fig. 5. Scheme of subsets pair location (blue squares) used for the determination of CTOD measurements.

Differentiating Eq. (6), the tractions can be directly defined as,

$$\sigma(w) = \frac{\mathrm{d}G_{\mathrm{I}}}{\mathrm{d}w}. \tag{7}$$

To apply this methodology, it is necessary to determine the evolution of strain energy release rate in mode I (G_{I}) as a function of the crack tip opening displacements (CTOD). In this work, the evolution of G_{I} was found from Eq. (5) and CTOD was directly monitored using the ARAMIS 3D DIC system. The CTOD (w) was obtained by post-processing the recorded displacements. To this end, the pre-crack tip was identified at the initial stage image and pairs of facet pairs symmetrical to the fracture plane were carefully selected (Fig. 5). According to this each top subset (+1, +2, ...) was paired with its lower symmetrical (−1, −2, ...). Determination of the CTOD was always started using the subsets closest to the crack tip (+1 and −1) and then the next subsets were automatically selected sequentially until a subsets of facets is read in each of the test images successfully. It should be noted that the first subset of facets are typically rejected since they often contain erroneous measurements. These errors can be observed as discontinuities in $w-\delta$ curve. Moreover, each subset was verified to be on an opposite side of the crack during propagation since the crack growth could place them on the same side. Finally, w was determined for each loading step by evaluating the relative displacement between both subsets [38,39],

$$w = \left\| w^{+} - w^{-} \right\|, \tag{8}$$

where w^{+} and w^{-} are the displacement components perpendicular to the crack surface (Figure 6) associated with the subsets described above and $\|\cdot\|$ represents the Euclidean norm.

There are eventually several ways to carry out the numerical differentiation given in Eq. (7), with advantages and drawbacks. The approximation of a continuous function based on a least-square regression strategy has been successfully applied in other relevant research available in literature (e.g. [11,13,40,41]) and is adopted in this work. To obtain σ, a logistic function was fitted to $G_{\mathrm{I}} - w$ curve by least squares through successive approximations according to the next expression,

$$G_{\mathrm{I}} = \frac{A_1 - A_2}{1 + \left(w/w_0\right)^{p}} + A_2, \tag{9}$$

where A_1, A_2, w_0 and p are fitting constants by the regression analysis. This function does not have a particular physical meaning, however it is used as a tool to smooth the noise before deriving Eq. (7). In this way, σ can be determined as follows,

$$\sigma = -\frac{p\left(A_1 - A_2\right)\left(w/w_0\right)^{p-1}}{w_0\left(1 + \left(w/w_0\right)^{p}\right)^{2}}. \tag{10}$$

The A_2 parameter in Eqs (9) and (10) should provide an estimation of the critical strain energy release rate according to Eq. (11),

$$A_2 = \lim_{w\to\infty} G_{\mathrm{I}} = G_{\mathrm{Ic}}. \tag{11}$$

In alternative to the employment of a continuous function in a global fitting approach, a local least-square fitting algorithm can be used considering, for instance, a smoothing spline [42,43].

2.5. A three-linear cohesive law model

In order to validate the experimental procedure, 2D finite element analyses were performed using ABAQUS software. A plane stress analysis together with quadratic isoparametric 8-node (CPS8R) solid element were used to model the DCB test. The damage zone was implemented as a user subroutine of the ABAQUS software and using 6 nodes elements located at half-height of the specimen according to the scheme in Fig. 7. A total displacement (δ) of 16 mm was applied, which was introduced in increments no greater than 0.02 mm in order to obtain numerically stable crack growth and accurate results.

A three-linear cohesive law model with a bilinear softening relationship (Fig. 8) was implemented to reproduce the crack growth in Mode I according to the experimental tests. Recent research shows good agreements on the application of a trilinear cohesive law to simulate crack growth in wood [11,20,30].

Two different parts can be distinguished in this fracture behavior model. Firstly, an initial branch where the material behaves elastically until the maximum traction σ_{u} is attained for a corresponding crack opening in mode I (w_0). It is defined by Eq. (12),

$$\sigma = kw, \tag{12}$$

where k is the initial stiffness of the cohesive elements and is known as the penalty parameter. It normally takes a high value (10^6 N/mm^3) to avoid undesirable interpenetrations and difficulties to achieve the model convergence [44]. Although this penalty stiffness value reveals to be higher than the ones estimated in the cohesive laws obtained experimentally, it should be noted that the goal in this work is to properly address the softening region taking part after the local strength is achieved. In fact, the rigorous simulation of damage initiation and its propagation are the main objectives to achieve. In this context, the second part of the trilinear cohesive law (Fig. 8) represents the development of the FPZ and damage initiation (microcracking in the first descending branch and fiber-bridging in the last one) and so the material behaves in a non-linear way after the local strength (σ_{u}) is attained. This part is defined by three parameters: the ultimate traction (σ_{u}), the traction at which fiber-bridging appears (σ_1) and the corresponding crack opening (w_1). The ultimate crack growing is defined from the fracture energy G_{Ic}. The traction–separation relationships at this part of the law are established according to Eq. (13),

$$\sigma = (1-d)kw, \tag{13}$$

where d is the damage parameter, which is updated at each loading increment during the iterative process and is obtained from the cohesive law as a function of w. This parameter assumes the value of Eqs. (14) and (15), depending on the branch to which it belongs. In this sense, if $w_0 < w < w_1$ then,

$$d = 1 - \frac{w_0}{w\sigma_{\mathrm{u}}}\left[\frac{\sigma_1 - \sigma_{\mathrm{u}}}{w_1 - w_0}\left(w - w_0\right) + \sigma_{\mathrm{u}}\right], \tag{14}$$

and when $w_1 < w < w_{\mathrm{u}}$ then,

$$d = 1 - \frac{w_0}{w\sigma_{\mathrm{u}}}\left[\frac{\sigma_1\left(w - w_{\mathrm{u}}\right)}{\left(w_{\mathrm{u}} - w_1\right)}\right]. \tag{15}$$

It should be noted that knowing G_{Ic}, the ultimate crack tip separation can be obtained as follows,

$$w_u = \frac{2G_{\mathrm{Ic}} - \sigma_{\mathrm{u}}w_1 + \sigma_1 w_0}{\sigma_1}. \tag{16}$$

The values of the parameters defining the cohesive law are shown in Table 1, which correspond to the average values obtained in Section 3. Furthermore, in order to explain the scatter of wood properties and

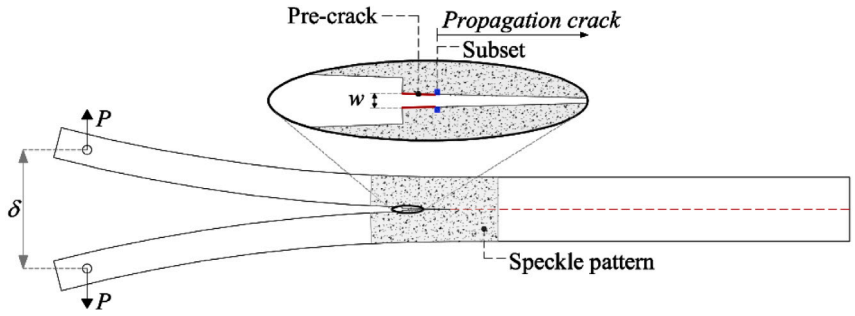

Fig. 6. Scheme of data measurement at the crack tip area of the specimen using DIC.

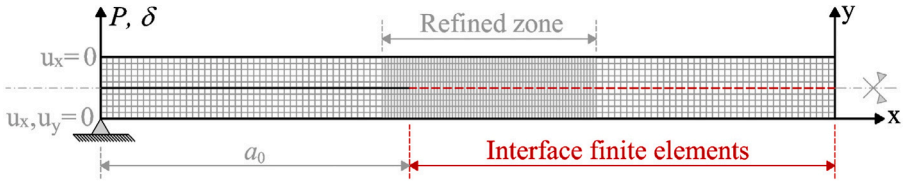

Fig. 7. Scheme of the numerical model and finite mesh.

Table 1
Numerical parameters of trilinear cohesive law. Maximum traction strength (σ_u), traction at which fiber-bridging appears (σ_1), displacement at which fiber-bridging appears (w_1) and critical fracture energy (G_{Ic}).

	σ_u (N/mm^2)	σ_1 (N/mm^2)	w_1 (mm)	G_{Ic} (kJ/m^2)	G_μ/G_{Ic} micro-cracking	G_b/G_{Ic} fiber-bridging
Average	8.29	1.00	0.080	0.46	70.28%	29.72%
upper limit	8.29	1.20	0.097	0.56	70.32%	29.68%
lower limit	8.29	0.80	0.063	0.36	70.23%	29.77%

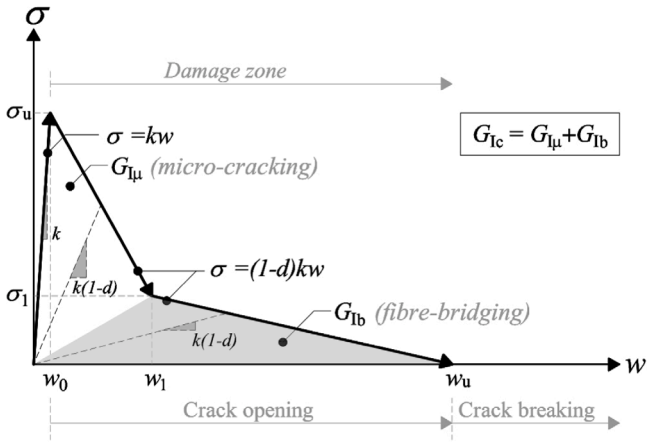

Fig. 8. Trilinear cohesive law.

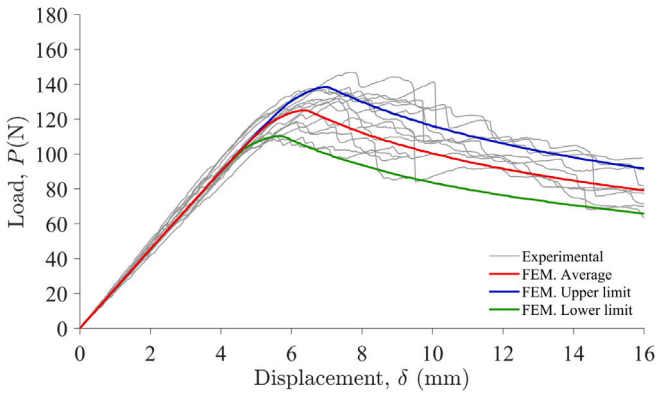

Fig. 9. Experimental and numerical $P-\delta$ curves from DCB test on beech.

knowing that the damage propagation is governed by the fracture energy, two additional cohesive laws have been implemented in FEM, representing the upper and lower limits of the fracture energy, whose values have been obtained by applying the St. Dev. to the mean value of G_{Ic}. It should be noted that these extreme cohesive laws were defined considering the same σ_u and keeping constant the proportionality between the micro-cracking and fiber-bridging fracture energy components obtained in the average cohesive law. This assumption relies on the fact that crack growth is essentially governed by fracture energy, not being much affected by σ_u.

The mean values of elastic constants of European beech used as input data in the numerical models were taken from [31] and are summarized in Table 2.

3. Results and discussion

3.1. R-Curves

Fig. 9 shows the $P-\delta$ curves obtained from the experimental DCB tests (in gray) and from the numerical analysis using the elastic constants specified in Table 2 and the fracture properties compiled in Table 1. The numerical curve derived using the average values of both elastic and fracture properties is shown in red, together with the numerical upper and lower limits by applying the standard deviation (St. Dev.) to the mean values (blue and green lines, respectively).

The experimental curves show consistent results taking into account the typical variability of wood. The numerical curve derived using the mean material properties is shown as representative of the experimental results. Furthermore, the upper and lower limit curves could explain

Table 2
Average elastic constants of European beech used as input data in the numerical models [31].

	E_L (MPa)	E_R (MPa)	E_T (MPa)	υ_{LR} (-)	υ_{LT} (-)	υ_{TR} (-)	G_{LR} (MPa)	G_{LT} (MPa)	G_{RT} (MPa)
Average	13811	1590	832	0.51	0.44	0.32	1108	706	349
St. Dev.	(1323)	(541)	(115)	(0.030)	(0.015)	(0.041)	(202)	(139)	(53)

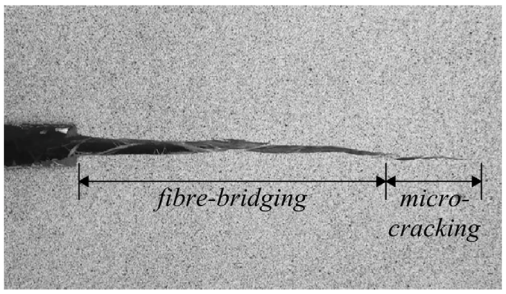

Fig. 10. Toughening mechanisms during crack propagation of the "*TL 06*" DCB specimen.

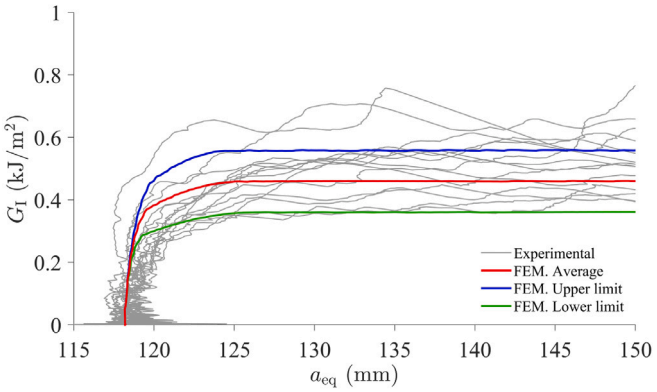

Fig. 11. *R*-curves from experimental DCB test in the TL propagation system and the numerical solutions.

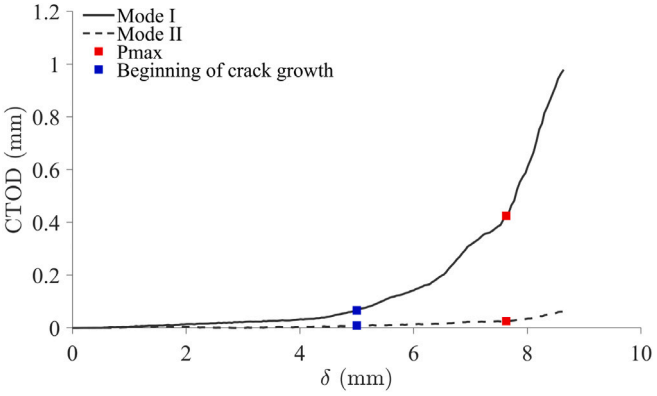

Fig. 12. Evaluation of the normal (Mode I) and parallel (Mode II) CTOD with regard to the applied displacement (δ).

the scatter of the wood properties. Accordingly, it is confirmed that finite element models using a trilinear cohesive law applied to CZM are a useful tool to predict the fracture behavior in mode I of beech. These statements are in agreement with other author's research using other wood species [11,45].

Non-linear behavior can be observed both in the experimental and numerical curves before the maximum load is attained. This is a typical feature of quasi-brittle materials like wood, due to the appearance of the aforementioned micro-cracking and fiber-bridging [13], as can be seen in Fig. 10. This fact verifies the existence of the FPZ ahead of the crack tip and therefore cannot be neglected. In addition, Fig. 10 reveals the difficulty of accurately monitoring crack growth during the tests, which supports the convenience of applying the CBBM scheme based on the equivalent crack length concept to assess the fracture energy [46].

The straight branch of the $P-\delta$ curves was used to calibrate the initial compliance (C_0), which was fitted by linear regression performed with Matlab® attaining coefficients of determination $R^2 > 0.999$. This value, together with the additional crack length ($a = a_0 + \delta$), were used to fit the corrected flexural modulus (E_f) and thus avoid measurement of this property in each DCB tests. The results for both C_0, E_f and maximum load (P_{max}) obtained for each DCB tests in addition to the mean, standard deviation (St. Dev.) and coefficient of variation (CoV) values are shown in Table 3. In the numerical models, an average value of E_L was used as input data, which seems to be quite consistent with the experimental tests as could be observed in Fig. 9. The dispersion of the results is within the expected range in wood.

The *R*-curves obtained from both experimental and numerical $P-\delta$ curves are shown in Fig. 11. These curves describe the evolution of the energy release rate (G_I) as a function of the equivalent crack length (a_{eq}), both parameters derived by applying the CBBM.

The scatter between curves is due to the typical wood variability. Overall, the G_I grows vertically until it steadies at a point represented by the plateau of the curves. This plateau indicates the critical fracture energy (G_{Ic}) and match to the beginning of the material damage, and therefore to the crack growth. A non-linear transition can be observed between the vertical and the horizontal part representing the development of the FPZ. However, in all cases, a plateau can be clearly seen in the *R*-curves, which shows a stable crack growth and therefore justifies the application of the proposed method. Given the length and dispersion of the points that generate the plateau of the *R*-curves, the G_{Ic} value was determined as the average value of the points that belong to this horizontal branch. The results are included also in Table 3. It should be highlighted that the numerical *R*-curves (average, upper limit and lower limit) obtained from the numerical $P-\delta$ fit quite well with the experimental results. Therefore, the use of cohesive elements to model the onset and evolution of damage seems to be a useful and simple tool whose applicability in beech wood (*Fagus sylvatica* L.) has been demonstrated.

The mean value of G_{Ic} (TL) for *Fagus sylvatica* L. resulted in 0.46 kJ/m^2 (22.1% COV). This value is higher than that of softwood species such as Picea abies, which according to [20] has a G_{Ic} value of 0.301 kJ/m^2. However, it is lower than the value obtained for other hardwoods species such as *Eucalyptus globulus* L., which applying the same methodology showed a G_{Ic} value of 0.77 kJ/m^2 according to [13].

3.2. Cohesive laws

The cohesive laws were determined from G_I (applying the CBBM) and the CTOD (w) measured using the DIC technique. In order to identify the eventual presence of spurious mode II loading, the evolution of CTOD (the normal component to the crack plane (Mode I) and the parallel component to the propagation system (Mode II)) with regard to the applied displacement (δ) for a representative experimental test is shown in Fig. 12.

As can be seen in the figure, the displacements belonging to Mode II are negligible. Therefore, the use of DCB specimens loaded in the

Table 3
Density (ρ), corrected flexural modulus (E_f), maximum load (P_{max}), initial compliance (C_0) and critical fracture energy (G_{Ic}) for each DCB specimen, and mean, standard deviation (St. Dev.) and coefficient of variation (CoV) values.

Specimen Ref	ρ (kg/m^3)	E_f (N/mm^2)	P_{max} (N)	C_0 (mm/N)	G_{Ic} (kJ/m^2)
TL_01	696	13500	108.74	0.044	0.36
TL_02	713	12914	134.70	0.048	0.45
TL_05	774	13283	146.95	0.046	0.65
TL_06	689	14797	132.09	0.042	0.49
TL_07	722	15375	135.19	0.041	0.44
TL_08	700	13817	129.97	0.044	0.51
TL_09	710	13164	108.74	0.045	0.34
TL_10	738	15183	136.50	0.041	0.54
TL_12	699	14804	118.70	0.043	0.27
TL_14	676	14735	110.05	0.044	0.35
TL_15	683	16012	138.95	0.041	0.53
TL_16	678	15536	131.93	0.042	0.52
TL_17	691	14910	118.37	0.044	0.41
TL_20	690	16524	137.64	0.040	0.51
Mean	**704**	**14611**	**127.75**	**0.043**	**0.46**
St. Dev.	26	1115	12.46	0.002	0.10
CoV (%)	3.7%	7.6%	9.8%	5.1%	22.1%

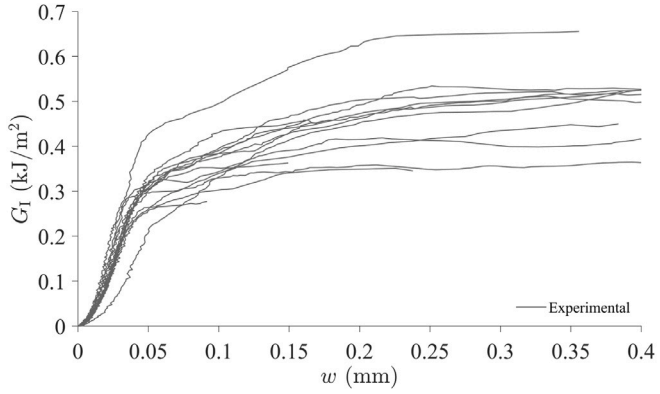

Fig. 13. Experimental $G_I - w$ curves.

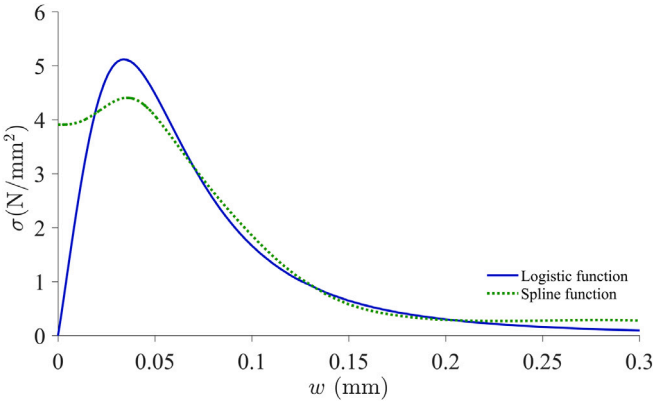

Fig. 15. Logistic and spline cohesive laws obtained for the "*TL 07*" DCB specimen.

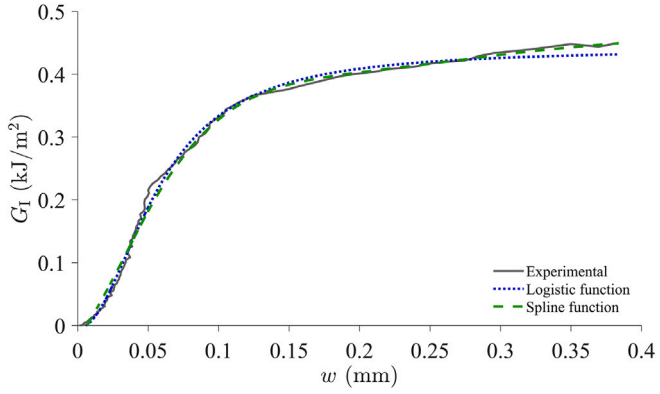

Fig. 14. Logistic and spline function fitting to the experimental $G_I - w$ curve obtained for the "*TL 07*" DCB specimen.

direction perpendicular to the grain seems to be a good test setup to determine G_{Ic} since the influence of mode II is very low.

The $G_I - w$ curves from the experimental tests are shown in Fig. 13. In order to have a continuous function that can be derived to obtain the cohesive laws, during data processing, both a logistic type function (Eq. (9)) and a spline type function were fitted. A representative example of this fit is shown in Fig. 14, which shows a good approximation of both functions. Nonetheless, it can be observed that the spline function fits better to the experimental curve due to its degrees of freedom. However, it has the disadvantage of being quite stiff at the beginning. Fig. 15 shows a representative example of the cohesive law obtained for each function. In this figure it can be seen how the spline function presents problems at the beginning due to the initial stiffness mentioned above. Therefore, in this study the cohesive laws were determined from the logistic function, since it proves to be a smoother and continuous function. It should be noted that only the data points from the start of the test to the beginning of crack propagation have been taken into account, since that point corresponds to the critical fracture energy.

All the experimental and the average cohesive laws of beech are shown in Fig. 16. The corresponding fitting parameters (A_1, A_2, w_0, p) of the logistic curves according to Eq. (10), the maximum traction (σ_u), fracture energy of the cohesive law ($G_{law,I}$) and maximum relative displacement (w_u) are summarized in Table 4. In particular, A_2 value is an estimate of G_{Ic}, which can be verified by comparing these values with those determined from the experimental R-curves shown in Table 3. It is also interesting to note that the σ_u values obtained from the cohesive laws are in agreement with the perpendicular tensile strength value in the tangential direction of 8.9 MPa for beech reported in the literature [47].

Table 4
Fitting parameters of the logistic function (A_1, A_2, w_0, p), maximum traction (σ_u), fracture energy ($G_{law,I}$) and maximum relative displacement (w_u) of the cohesive laws for each DCB specimen. Mean, standard deviation (St. Dev.) and coefficient of variation (CoV) values.

Specimen Ref	A_1 (kJ/m^2)	A_2 (kJ/m^2)	w_{10} (mm)	**p** (-)	$G_{law,I}$ (kJ/m^2)	σ_u (N/mm^2)	w_u (mm)
TL_01	0.007	0.35	0.029	3.12	0.34	10.07	0.024
TL_02	0.003	0.46	0.034	2.42	0.45	9.65	0.024
TL_05	−0.002	0.61	0.036	2.18	0.61	11.41	0.023
TL_06	−0.009	0.49	0.047	1.51	0.50	6.56	0.016
TL_07	−0.004	0.44	0.057	2.06	0.44	5.12	0.034
TL_08	−0.013	0.51	0.041	1.64	0.51	7.81	0.018
TL_09	0.008	0.35	0.024	3.16	0.34	12.57	0.020
TL_10	−0.023	0.54	0.045	1.45	0.55	7.72	0.014
TL_12	0.008	0.29	0.026	3.25	0.28	9.76	0.021
TL_14	0.004	0.33	0.031	2.48	0.33	7.83	0.022
TL_15	−0.013	0.53	0.043	1.66	0.53	7.71	0.019
TL_16	−0.020	0.52	0.040	1.43	0.53	8.21	0.012
TL_17	−0.009	0.39	0.026	2.04	0.40	10.10	0.015
TL_20	−0.007	0.51	0.042	1.84	0.51	7.77	0.022
Mean	**−0.005**	**0.46**	**0.037**	**2.16**	**0.46**	**8.74**	**0.020**
St. Dev.	0.010	0.09	0.009	0.64	0.10	1.97	0.005
CoV (%)	–	20.9%	25.5%	29.8%	21.3%	22.5%	27.1%

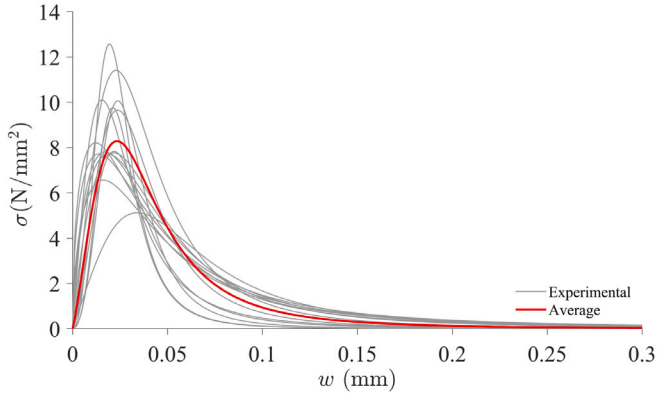

Fig. 16. Experimental cohesive laws (in gray) and average cohesive law (in red) in mode I for beech.

4. Conclusions

The *R*-curves and the cohesive laws in mode I and TL crack propagation system were determined for European beech by means of DCB tests. To derive G_I, the CBBM data reduction scheme, based on beam theory and equivalent crack length concept (a_{eq}), was applied. This method only requires the monitoring of the $P-\delta$ curve, which is an advantage relative to classical procedures. The CTOD (w) was measured directly by the DIC technique. A logistic function was fitted to the $G_I.-w$ curves to obtain the cohesive laws after differentiation of this relation. A mean G_{Ic} value of 0.46 kJ/m^2 was determined for this hardwood species. Furthermore, the mean σ_u value of 8.74 N/mm^2 obtained from the average cohesive law is consistent with the perpendicular tensile strength available in the literature.

The methodology proposed in this work was validated by finite elements model implementing a mean trilinear cohesive law with a bilinear softening relationship using CZM to simulate the crack growth under loads in Mode I. Two additional cohesive laws corresponding to the upper and lower limits of the critical fracture energy were proposed, resulting in a band capable of representing the scatter of wood properties in a simple way. The fracture properties obtained are fundamental to develop reliable numerical models for timber engineering design purposes using European beech.

CRediT authorship contribution statement

J.L. Gómez-Royuela: Conceptualization, Methodology, Software, Validation, Formal analysis, Investigation, Resources, Writing – original draft, Writing – review & editing.. **A. Majano-Majano:** Conceptualization, Methodology, Investigation, Resources, Writing – review & editing, Supervision, Funding acquisition. **A.J. Lara-Bocanegra:** Conceptualization, Methodology, Investigation, Resources, Writing – review & editing, Supervision. **J. Xavier:** Conceptualization, Methodology, Software, Validation, Resources, Writing – review & editing, Supervision, Funding acquisition. **M.F.S.F. de Moura:** Conceptualization, Methodology, Software, Validation, Resources, Writing – review & editing, Supervision, Funding acquisition.

Declaration of competing interest

The authors declare that they have no known competing financial interests or personal relationships that could have appeared to influence the work reported in this paper.

Acknowledgments

Part of the work was undertaken during a short-term scientific stay by the first author at the Faculty of Engineering (University of Porto) in 2021, with the financial support of *Programa Propio de I+D+i 2021 de la Universidad Politécnica de Madrid*. The authors acknowledge Fundação para a Ciência e a Tecnologia (FCT-MCTES) for the financial support of the *Laboratório Associado de Energia*, Transportes e Aeronáutica (LAETA) by the project UID/EMS/50022/2019 and the Research and Development Unit for Mechanical and Industrial Engineering (UNIDEMI) by the project UIDB/00667/2020.

References

[1] UNEP, Buildings and climate change. Summary for decision-makers, United Nation Environ. Programme (2009) 1–62.
[2] L. Gustavsson, R. Sathre, Variability in energy and carbon dioxide balances of wood and concrete building materials, Build. Environ. 41 (7) (2006) 940–951.
[3] L.O. Eriksson, L. Gustavsson, R. Hänninen, M. Kallio, H. Lyhykäinen, K. Pingoud, J. Pohjola, R. Sathre, B. Solberg, J. Svanaes, L. Valsta, Climate change mitigation through increased wood use in the European construction sector-towards an integrated modelling framework, Eur. J. Forest Res. 131 (1) (2012) 131–144.
[4] A.H. Buchanan, S.B. Levine, Wood-based building materials and atmospheric carbon emissions, Environ. Sci. Policy 2 (6) (1999) 427–437.
[5] A.H. Buchanan, B.G. Honey, Energy and carbon dioxide implications of building construction, Energy Build. 20 (3) (1994) 205–217.
[6] T. Ehrhart, European Beech glued laminated timber, 2019, 26173.
[7] European Committee for Standardization (CEN), EN 1995-1-1:2004 design of timber structures. Brussels, Belgium, 2016.
[8] T.A.C.M. Van der Put, A.J.M. Leitjen, Evaluation of perpendicular to grain failure of beams caused by concentrated loads of joints, CIB-W18, Meeting Thirty-Three, Paper 33-7-7, Delft, The Netherlands, 2000.

[9] T.A.C.M. Van der Put, Tension perpendicular to the grain at notches and joints, in: Proceedings Of CIB-W18 Conference, Paper 23-10-1, Lisbon, Portugal., 1990.
[10] J. Xavier, P. Monteiro, J.J. Morais, N. Dourado, M.F. De Moura, Moisture content effect on the fracture characterisation of *Pinus pinaster* under mode I, J. Mater. Sci. 49 (21) (2014) 7371–7381.
[11] J. Xavier, M. Oliveira, P. Monteiro, J.J. Morais, M.F. de Moura, Direct evaluation of cohesive law in mode I of *Pinus pinaster* by digital image correlation, Exp. Mech. 54 (5) (2014) 829–840.
[12] N.M. Dourado, M.F. De Moura, J.J. Morais, M.A. Silva, Estimate of resistance-curve in wood through the double cantilever beam test, Holzforschung 64 (1) (2010) 119–126.
[13] A. Majano-Majano, A.J. Lara-Bocanegra, J. Xavier, J. Morais, Measuring the cohesive law in mode I loading of *Eucalyptus globulus*, Materials 12 (1) (2019) 23.
[14] R.A. Luimes, A.S. Suiker, C.V. Verhoosel, A.J. Jorissen, H.L. Schellen, Fracture behaviour of historic and new oak wood, Wood Sci. Technol. 52 (5) (2018) 1243–1269.
[15] Y. Yu, R. Xin, W. Zeng, W. Liu, Fracture resistance curves of wood in the longitudinal direction using digital image correlation technique, Theor. Appl. Fract. Mech. 114 (2021) 102997.
[16] K. Ostapska, K.A. Malo, Crack path tracking using DIC and XFEM modelling of mixed-mode fracture in wood, Theor. Appl. Fract. Mech. 112 (January) (2021).
[17] M.F. de Moura, N. Dourado, Mode I fracture characterization of wood using the TDCB test, Theor. Appl. Fract. Mech. 94 (September 2017) (2018) 40–45.
[18] A. Majano-Majano, M. Hughes, J.L. Fernandez-Cabo, The fracture toughness and properties of thermally modified beech and ash at different moisture contents, Wood Sci. Technol. 46 (2012) 5–21.
[19] M. Merhar, D.G. Bučar, B. Bučar, Faktor kritičnog intenziteta naprezanja (i. mod) bukovine (*Fagus sylvatica*) u TL presjeku: Usporedba različitih metoda, Drvna Ind. 64 (3) (2013) 221–229.
[20] N. Dourado, M.F. de Moura, S. Morel, J. Morais, Wood fracture characterization under mode I loading using the three-point-bending test. Experimental investigation of *Picea abies l.*, Int. J. Fract. 194 (2015) 1–9.
[21] A. Reiterer, G. Sinn, S.E. Stanzl-Tschegg, Fracture characteristics of different wood species under mode I loading perpendicular to the grain, Mater. Sci. Eng. A 332 (1–2) (2002) 29–36.
[22] S.E. Stanzl-Tschegg, D.M. Tan, E.K. Tschegg, New splitting method for wood fracture characterization, Wood Sci. Technol. 29 (1) (1995) 31–50.
[23] H. Yoshihara, T. Kawamura, Mode I fracture toughness estimation of wood by DCB test, Composites A 37 (11) (2006) 2105–2113.
[24] M.F. de Moura, J.J. Morais, N. Dourado, A new data reduction scheme for mode I wood fracture characterization using the double cantilever beam test, Eng. Fract. Mech. 75 (13) (2008) 3852–3865.
[25] D.S. Dugdale, Yielding of steel, J. Mech. Phys. Solids 8 (1960) 100–104.
[26] A. Hillerborg, M. Modéer, P.-E. Petersson, Analysis of crack formation and crack growth in concrete by means of fracture mechanics and finite elements, Cem. Concr. Res. 6 (1976) 773–782.
[27] P.-E. Petersson, Crack Growth and Development of Fracture Zones in Plain Concrete and Similar Materials, Report TVBM, Division Of Building Materials, Lund Institute Of Technology, Lund, Sweden, 1981.
[28] L. Boström, Method of determination of the softening behaviour of wood and the applicability of a nonlinear fracture mechanics model, Lund (PhD thesis), (TVBN-1012) 1992, p. 148.
[29] L. Boström, The stress-displacement relation of wood perpendicular to the grain - part 1. Experimental determination of the stress-displacement relation, Wood Sci. Technol. 28 (4) (1994) 309–317.
[30] N. Dourado, S. Morel, M.F. de Moura, G. Valentin, J. Morais, Comparison of fracture properties of two wood species through cohesive crack simulations, Composites A 39 (2) (2008) 415–427.
[31] J.L. Gómez-Royuela, A. Majano-Majano, A.J. Lara-Bocanegra, T.P.S. Reynolds, Determination of the elastic constants of thermally modified beech by ultrasound and static tests coupled with 3D digital image correlation, 302, 302 (2021) 124270.
[32] GOM mbH, ARAMIS Commercial software. Aramis 6.0.2; GOM mbH: Braunschweig, Germany, 2007.
[33] J. Xavier, A. de Jesus, J. Morais, J. Pinto, Stereovision measurements on evaluating the modulus of elasticity of wood by compression tests parallel to the grain, Constr. Build. Mater. 26 (1) (2012) 207–215.
[34] J. Pereira, J. Xavier, B. Ghiassi, J. Lousada, J. Morais, On the identification of earlywood and latewood radial elastic modulus of pinus pinaster by digital image correlation: A parametric analysis, J. Strain Anal. Eng. Des. 53 (8) (2018) 566–574.
[35] J. Williams, The fracture mechanics of delamination tests, 1989.
[36] F.A. Pereira, J.J. Morais, M.F. de Moura, N. Dourado, M.I. Dias, Evaluation of bone cohesive laws using an inverse method applied to the DCB test, Eng. Fract. Mech. 96 (2012) 724–736.
[37] J.R. Rice, A path independent integral and the approximate analysis of strain concentration by notches and cracks, J. Appl. Mech. Trans. ASME 35 (2) (1968) 379–388.
[38] A.M. Sousa, J. Xavier, J.J. Morais, V.M. Filipe, M. Vaz, Processing discontinuous displacement fields by a spatio-temporal derivative technique, Opt. Lasers Eng. 49 (12) (2011) 1402–1412.
[39] J. Xavier, A.M.R. Sousa, J.J.L. Morais, V.M.J. Filipe, M. Vaz, Measuring displacement fields by cross-correlation and a differential technique: experimental validation, Opt. Eng. 51 (4) (2012) 043602.
[40] J. Xavier, J.R. Fernandes, O. Frazão, J.J. Morais, Measuring mode I cohesive law of wood bonded joints based on digital image correlation and fibre bragg grating sensors, Compos. Struct. 121 (2015) 83–89.
[41] J. Oliveira, J. Xavier, F. Pereira, J. Morais, M. de Moura, Direct evaluation of mixed mode I+II cohesive laws of wood by coupling MMB test with DIC, Materials 14 (2) (2021) 374.
[42] F. Pereira, M. de Moura, N. Dourado, J. Morais, J. Xavier, M. Dias, Direct and inverse methods applied to the determination of mode I cohesive law of bovine cortical bone using the DCB test, Int. J. Solids Struct. 128 (2017) 210–220.
[43] F. Silva, M. de Moura, N. Dourado, J. Xavier, F. Pereira, J. Morais, M. Dias, Mixed-mode I+II fracture characterization of human cortical bone using the single leg bending test, J. Mech. Behav. Biomed. Mater. 54 (2016) 72–81.
[44] C.G. Dávila, P.P. Camanho, M.F. De Moura, Mixed-mode decohesion elements for analyses of progressive delamination, in: 19th AIAA Applied Aerodynamics Conference, May 2014, 2001.
[45] N. Dourado, M.F. de Moura, Effect of temperature on the fracture toughness of wood under mode I quasi-static loading, Constr. Build. Mater. 223 (2019) 863–869.
[46] J. Xavier, J. Morais, N. Dourado, M.F. De Moura, Measurement of mode I and mode II fracture properties of wood-bonded joints, J. Adhes. Sci. Technol. 25 (20) (2012) 2881–2895.
[47] T. Ozyhar, S. Hering, P. Niemz, Moisture-dependent elastic and strength anisotropy of European beech wood in tension, J. Mater. Sci. 47 (16) (2012) 6141–6150.